Classification of accidental band crossings and emergent semimetals in two-dimensional noncentrosymmetric systems

Sungjoon Park and Bohm-Jung Yang*

Department of Physics and Astronomy, Seoul National University, Seoul 08826, Korea;
Center for Correlated Electron Systems, Institute for Basic Science (IBS), Seoul 08826, Korea;
and Center for Theoretical Physics (CTP), Seoul National University, Seoul 08826, Korea

(Received 24 April 2017; revised manuscript received 18 August 2017; published 18 September 2017)

We classify all possible gap-closing procedures which can be achieved in two-dimensional time-reversal invariant noncentrosymmetric systems. For exhaustive classification, we examine the space-group symmetries of all 49 layer groups lacking inversion, taking into account spin-orbit coupling. Although a direct transition between two insulators is generally predicted to occur when a band crossing happens at a general point in the Brillouin zone, we find that a variety of stable semimetal phases with point or line nodes can also arise due to the band crossing in the presence of additional crystalline symmetries. Through our theoretical study, we provide the complete list of nodal semimetals created by a band inversion in two-dimensional noncentrosymmetric systems with time-reversal invariance. The transition from an insulator to a nodal semimetal can be grouped into three classes depending on the crystalline symmetry. First, in systems with a twofold rotation about the z axis (normal to the system), a band inversion at a generic point generates a two-dimensional Weyl semimetal with point nodes. Second, when the band crossing happens on the line invariant under a twofold rotation (mirror) symmetry with the rotation (normal) axis lying in the two-dimensional plane, a Weyl semimetal with point nodes can also be obtained. Finally, when the system has a mirror symmetry about the plane embracing the whole system, a semimetal with nodal lines can be created. Applying our theoretical framework, we identify various two-dimensional materials as candidate systems in which stable nodal semimetal phases can be induced via doping, applying electric field, or strain engineering, etc.

DOI: 10.1103/PhysRevB.96.125127

I. INTRODUCTION

Recent discovery of three-dimensional (3D) Dirac [1–12] and Weyl [13–21] fermions in condensed matter has triggered intensive research in semimetals with point or line nodes, dubbed nodal semimetals (NSM). Broadly, NSMs can be grouped into two classes. In the first class, the degeneracy at the band crossing point/line is enforced by the nonsymmorphic space-group symmetry of the system. In this class of NSMs, a certain minimal number of bands are required to stick together. Thus the presence of nodal points/lines at the Fermi level can be guaranteed by the electron filling [22]. On the other hand, in the second class of NSMs, the gap-closing points/lines are created via a band inversion, that is, through a transition from an insulator to a semimetal via an accidental band crossing (ABC). In this class of NSMs, the location of nodal points/lines in the momentum space varies depending on external parameters such as pressure, chemical doping, etc. Here each nodal point/line carries a quantized topological charge, which guarantees the stability of NSMs [6,8,23–25]. In the case of semimetals with point nodes belonging to this class, a pair-creation/pair-annihilation of nodal points can even mediate topological quantum phase transitions between two insulators [5,24,25].

In contrast to 3D, it is generally more difficult to have stable NSMs in two dimensions (2D) due to the lower dimensionality. For instance, even the well-known Dirac fermions in graphene become unstable, and thus gapped, once spin-orbit coupling (SOC) is included [26,27]. Recently, several interesting ideas have been proposed to stabilize 2D NSMs by using nonsymmorphic crystalline symmetries, thus leading to symmetry-enforced NSMs [28,29]. However, there has been no systematic study yet on the other class of 2D NSMs created via a band inversion. Considering that the band gap of 2D systems is easier to control than that of 3D systems via gating or strain engineering, it is essential to understand the outcome of a band inversion and the nature of resulting NSMs for future device application as well as for its fundamental physical aspect.

In this paper, we classify all possible ABC events in time-reversal invariant 2D noncentrosymmetric systems. For exhaustive investigation of ABCs and the resultant semimetals, we use a group theoretical approach by considering all possible layer groups (LGs) with broken inversion symmetry including SOC. We have found that there are three different types of ABC events as summarized in Fig. 1. In the first type, there is a direct transition between two insulators. In the second type, a band inversion creates a 2D Weyl semimetal with point nodes. We will call such twofold degenerate point nodes with linear dispersion "Weyl" points (WPs) instead of two-dimensional "Dirac" points, which we reserve for fourfold degenerate point nodes with linear dispersion. Finally, in the third type, a nodal line semimetal is created by a band inversion. At the critical point between an insulator and its neighboring phase, one can find characteristic fermionic excitations which lead to novel quantum critical behaviors. We propose various 2D materials in which our theory can be tested by engineering the electronic band structure.

The rest of this paper is organized as follows. In Sec. II we give a complete classification of a gap-closing pattern, which is summarized in Table I, and the $\mathbf{k}\cdot\mathbf{p}$ Hamiltonian at the quantum

*bjyang@snu.ac.kr

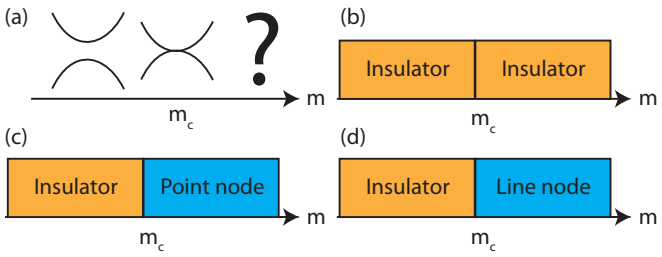

FIG. 1. (a) Possible phase diagrams achieved by an ABC in time-reversal invariant 2D noncentrosymmetric systems. (b) An insulator-to-insulator transition when there is no additional symmetry at the gap-closing point. (c) Transition from an insulator to a semimetal with point nodes occurring when the system has either a twofold rotation $C_{2x,2y,2z}$ or a mirror $M_{x,y}$. (d) Transition from an insulator to a semimetal with line nodes occurring when the system has a mirror M_z.

critical point. In Sec. III, we briefly discuss the topological charges that protect the nodal semimetallic phases in Sec. II. In Sec. IV, we explain how our classification scheme can be used, which is followed by discussion in Sec. V. In Appendix A, we give a detailed derivation of the $\mathbf{k}\cdot\mathbf{p}$ Hamiltonian presented in Sec. II. In Appendix B, we discuss how consideration of time-reversal symmetry affects degeneracy of bands, which must be known for the derivation of the classification scheme in Sec. II. In Appendix C, we discuss the topological phase transition that may be expected in black phosphorous in the perspective of our theory. Finally, in Appendix D, we explain the labels used for the high-symmetry points and lines in the two-dimensional Brillouin zones.

II. CLASSIFICATION OF ABC EVENTS IN LAYER GROUPS

Our strategy for classifying ABC events is as follows. In the absence of inversion symmetry, energy bands are generally nondegenerate at a generic momentum $\boldsymbol{k}$. Thus, the relevant symmetry group at $\boldsymbol{k}$, the $\boldsymbol{k}$ group hereafter, would have a one-dimensional irreducible representation (1D irrep). In such cases, the ABC at $\boldsymbol{k}_0$ between two nondegenerate bands can be described by a 2×2 Hamiltonian,

$$H(\mathbf{q},m) = f_0(\boldsymbol{q},m) + \sum_{i=1,2,3} f_i(\boldsymbol{q},m)\sigma_i, \qquad (1)$$

where σ_i are the Pauli matrices describing the two bands and $f_{0,1,2,3}$ are real functions of the momentum $\boldsymbol{q} = \boldsymbol{k} - \boldsymbol{k}_0$ and an external parameter m representing pressure, doping, etc. Here one can ignore f_0 as it does not contribute to the band gap. On the other hand, as discussed more fully in Appendix B, one may expect a band degeneracy associated with a higher dimensional irrep at some high-symmetry lines or points, such as a time-reversal invariant momentum (TRIM) [30]. However, since the bands degenerate at $\boldsymbol{k}_0$ generally disperse linearly away from $\boldsymbol{k}_0$, the band minimum or maximum is located away from $\boldsymbol{k}_0$, which means that an ABC always happens away from $\boldsymbol{k}_0$. Thus, we can limit ourselves to the case where the irrep of the conduction and the valence bands, R_c and R_v, respectively, are one dimensional with the effective Hamiltonian in Eq. (1) [31].

TABLE I. Classification table of all possible gap-closing patterns for 49 inversion asymmetric layer groups (LGs). The first column indicates the LG numbers used in Ref. [37]. The second column denotes the corresponding space group. When there are multiple groups sharing the same gap-closing pattern, the LG and the corresponding space group are listed in the same order. The third column describes gap-closing patterns.

Layer group	Space group	Gap-closing pattern
1, **65**	**1**, **143**	**f**
3, **49**, **50**, **73**	**3**, **75**, **81**, **168**	**1p**
4, **5**, **27**, **28**, **29**, **30**, **35**, **36**, **74**, **78**, **79**	**6**, **7**, **25**, **26**, **26**, **27**, **35**, **39**, **174**, **187**, **189**	ij:**loop**
31, **32**, **33**, **34**	**28**, **31**, **29**, **30**	ij:**loop**; ⟨4⟩:**loop**,**1l** DA, D
8, **9**	**3**, **4**	ij:**1l** Δ, TA, D, DA
10	**5**	ij:**1l** DA, Δ, FA, F
11, **12**,**13**	**6**, **7**, **8**	ij:**1l** SN,Σ,CA,C
19, **23**	**16**, **25**	**1p**; ii,ij:**1s**,**1l** Δ, D, Σ, C
20	**17**	**1p**; ii,ij:**1s**,**1l** Δ, D, Σ
24	**28**	**1p**; ii,ij:**1s**,**1l** Δ, Σ, C
21, **25**, **54**, **56**, **58**	**18**, **32**, **90**, **100**, **113**	**1p**; ii,ij:**1s**,**1l** Δ, Σ
60	**117**	**1p**; ii,ij:**1s**,**1l** Δ, Σ
22, **26**	**21**, **35**	**1p**; ii,ij:**1s**,**1l** Σ, Δ, F, C
53, **55 57**, **59**	**89**, **99**, **111**, **115**	**1p**; ii,ij:**1s**,**1l** Δ, Σ, Y
67, **69**	**149**, **156**	ij:**1l** Σ, SN
68, **70**	**150**, **157**	ij:**1l** Λ, T, TA, LE; ij:**3l** K, KA
76, **77**	**177**, **183**	**1p**; ii,ij:**1s**,**1l** Λ, Σ, T; ij:**3l** K

Since the symmetry of a 2D crystal embedded in a 3D space is described by a layer group, one can exhaustively classify all possible ABC events in 2D by analyzing the 49 inversion asymmetric LGs in the presence of SOC.

Suppose that the band gap of a system which can be tuned by varying m stays finite for $m < m_c$ but closes at $m = m_c$. We are interested in the nature of this system when $m > m_c$. To describe an ABC at a generic momentum $\mathbf{k}_0$, three equations $f_{1,2,3} = 0$ must be satisfied. Since we have three parameters (k_x,k_y,m), we expect a unique solution near the critical point. Such a solution describes the critical point between two insulators, as illustrated in Fig. 1(b). However, when the $\boldsymbol{k}$ group at the gap-closing point $\boldsymbol{k}_0$ has certain crystalline symmetries that impose constraints on $f_{1,2,3}$, the gap-closing condition can be modified, leading to NSM when $m > m_c$. Below, we list all symmetries in a $\boldsymbol{k}$ group that give nontrivial solutions to the problem at hand. We work out the nonsymmorphic symmetry explicitly only in case [b] below, since a similar idea can be applied to the other cases.

[a] No symmetry: There is no constraint on $f_{1,2,3}$, thus one can find a unique gap-closing solution $(\boldsymbol{k}_0, m_c)$. In this case, an ABC occurs only through fine tuning. We label this process by **f**, representing fine tuning.

[b] Twofold rotation C_{2x} (similarly for C_{2y} or mirror M_x, M_y): (i) If $R_c = R_v$, we may take $C_{2x} = c\sigma_0$ where σ_0 is the 2×2 identity matrix and $|c| = 1$. Here c may be a function of $\mathbf{k}$ if we consider a nonsymmorphic counterpart of this symmetry. On a symmetry line, the Hamiltonian is as in Eq. (1), since C_{2x} does not give any further constraint. Thus, the gap-closing condition gives three equations whereas there are only two variables, that is, m and the momentum on the symmetry line. Thus, in general, the band gap cannot be closed on the symmetry line. (ii) If $R_c = -R_v$, we can write $C_{2x} = c\sigma_3$ so $H = f_3\sigma_3$ on the symmetry line. In this case, the gap-closing problem has two variables and one equation so the solution is one dimensional in the parameter space. We label this as **1l**, where **1** denotes the number of WP pairs created and **l** indicates the WPs are on the symmetry line [see Fig. 2(d)].

[c] $C_{2z}\Theta$: $C_{2z}\Theta$ is a local symmetry in the 2D momentum space. Since $C_{2z}\Theta$ is antiunitary, its general form is $C_{2z}\Theta = UK$, where K denotes complex conjugation and U indicates a unitary matrix. After a suitable unitary transformation, one can always have $C_{2z}\Theta = K$ as shown in Appendix B. Since $C_{2z}\Theta$ requires the Hamiltonian $H(\boldsymbol{k})$ to be real, $f_2 = 0$. Then the gap-closing condition gives two equations whereas there are three parameters. This means that the solution is one-dimensional, and this describes a creation of a WP pair and their evolution in the momentum space. We label this by **1p**, where **p** stands for the plane where WPs are located and **1** indicates the number of WP pairs. Let us note that we count the number of WP pairs locally. In fact, C_{2z} implies that there is another WP pair created at $-\boldsymbol{k}_0$ [see Fig. 2(b)]. Let us also note that in systems with $C_{2z}\Theta$, the Weyl semimetal is stable irrespective of the eigenvalues of the bands, since each WP carries a quantized π Berry phase [32,33].

[d] M_z: M_z is also a local symmetry in the 2D momentum space. (i) If $R_c = R_v$, only fine tuning gives 2D WPs since there are three equations and three variables. (ii) If $R_c = -R_v$, one can choose $M_z = \sigma_3$, which gives $H = f_3\sigma_3$. The gap-closing condition gives one equation while we have three parameters, so ABC occurs in a 2D manifold in the parameter space, which translates to the creation of a line node and its evolution. Since the gap-closing points, in general, form a loop in the momentum space, we label it by **loop** [see Fig. 2(a)].

[e] C_{2x} and $C_{2y}\Theta$ (similarly for C_{2y} and $C_{2x}\Theta$, or $M_{x(y)}$ and $M_{y(x)}\Theta$): Since $C_{2x}C_{2y}\Theta \propto C_{2z}\Theta$ ($M_xM_y\Theta \propto C_{2z}\Theta$), a WP is stable even when it is away from high-symmetry axes. (i) Considering C_{2x} eigenvalues, if $R_c = R_v$, $C_{2x} = i\sigma_0$ and the Hamiltonian is not constrained by C_{2x} on its invariant axis. However, due to $C_{2z}\Theta$, the Hamiltonian should be real. Then on the C_{2x} invariant axis, the gap-closing condition gives two equations with two parameters, including the momentum along the invariant axis and m, which leads to case **f** on the invariant axis. However, a more detailed analysis shows that the gap closing on the C_{2x} invariant axis creates a pair of WP that move symmetrically away from the invariant axis. We label this case as **1s** where **s** means symmetrical [see Fig. 2(c)]. (ii) If $R_c = -R_v$, one can choose $C_{2x} = i\sigma_3$. Then the Hamiltonian on the invariant axis depends only on f_3, and the gap-closing condition gives one equation with two parameters, which describes the creation of a WP pair following the pattern **1l**.

[f] C_{2x} and M_y: Since $C_{2x}M_y \propto M_z$, a nodal line can appear after a band inversion. Let us note that C_{2x} and M_y share the same invariant line. (i) If $\{C_{2x}, M_y\} = 0$ on the invariant line (recall that these can be nonsymmorphic), two bands with different C_{2x} (or M_y) eigenvalues are doubly degenerate. In this case, a band inversion does not happen on the invariant line. (ii) If $[C_{2x}, M_y] = 0$ on the invariant line, each band on the invariant line carries C_{2x} and M_y eigenvalues simultaneously. When a band inversion happens between two bands with different C_{2x} (M_y) eigenvalues while sharing the same M_y (C_{2x}) eigenvalues, a nodal line is created after the band inversion corresponding to a **loop**. If both C_{2x} and M_y eigenvalues are different between two bands, the band inversion creates a WP pair on the invariant line corresponding to **1l**.

[g] C_3 plus C_{2x} or M_y: This happens at the K or KA point of the hexagonal Brillouin zone. Since two bands with C_3 eigenvalues $e^{i\pi/3}$ and $e^{-i\pi/3}$, respectively, are degenerate at K or KA, a band inversion can happen only between two bands with C_3 eigenvalue -1. When these two bands carry different C_{2x} or M_y eigenvalues, a band inversion can happen and create three pairs of WPs, which are located on the lines invariant under C_{2x} or M_y. We label it **3l**, as shown in Fig. 2(e).

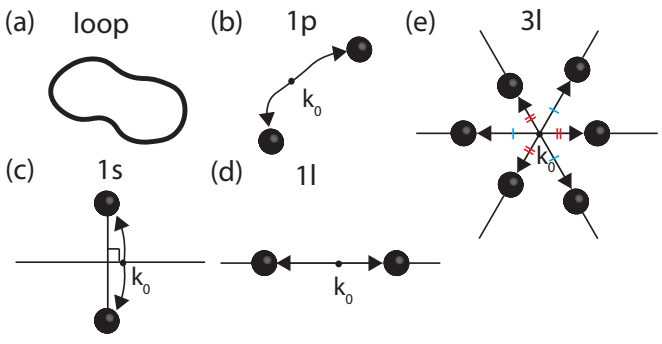

FIG. 2. Schematic figures describing the structure of gap-closing points created by a band inversion in 2D momentum space. (a) **loop**: A line node moves in the plane. (b) **1p**: A WP pair moves in the plane. (c) **1s**: A WP pair moves symmetrically with respect to a symmetry line. (d) **1l**: A WP pair moves along a symmetry line. (e) **3l**: Three pairs of WPs move along symmetry lines.

A. Classification table

We summarize all possible gap-closing patterns in Table I for 49 LGs lacking inversion symmetry. We list LG numbers in the first column and the corresponding space-group numbers in the second column. Note that for each LG L, there is a space group G such that if T(1) is a one-dimensional translation subgroup, $L \approx G/T(1)$ [34,35]. In the third column, we list the possible gap-closing patterns. Here we use the notation ii to mean $R_c = R_v$, and ij to mean $R_c \neq R_v$. We also use the notation ii:ij:**1s**,**1l** to mean ii leads to **1s** and ij leads to **1l**. ⟨4⟩:**loop**,**1l** is used for case [f] above, where there are four possible 1D irreps. In this case, different M_z eigenvalues lead to **loop** while different C_{2x} or M_y eigenvalues lead to **1l**. In

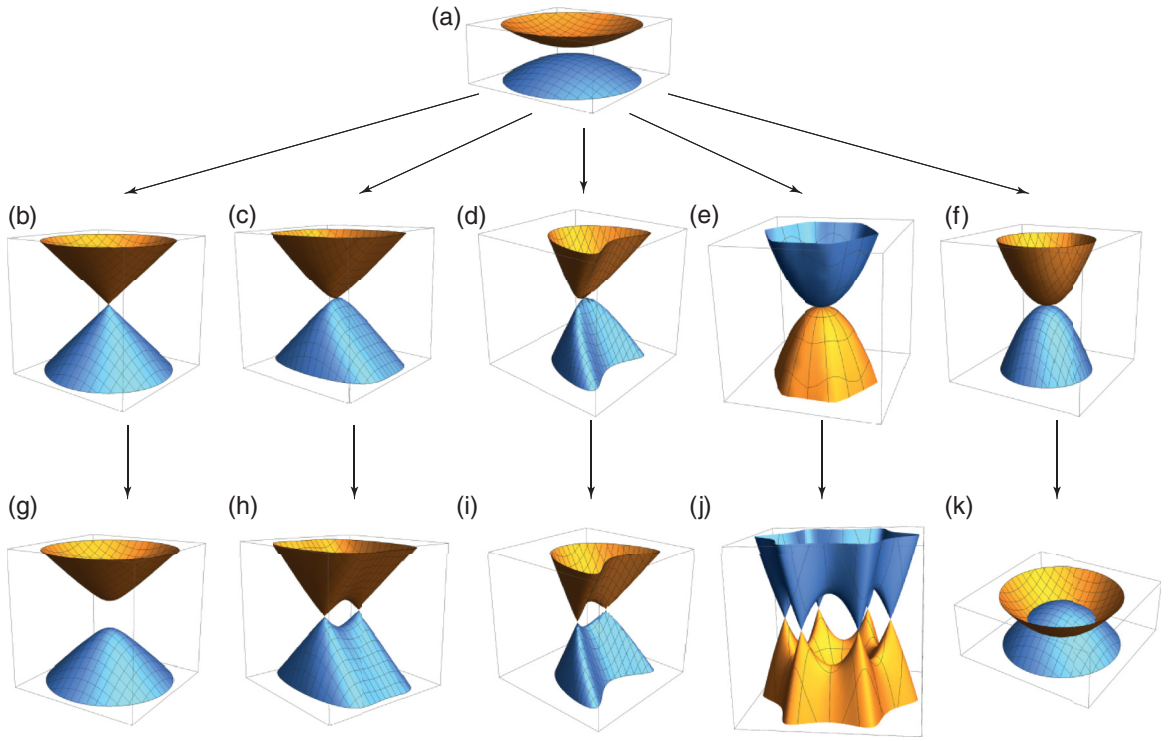

FIG. 3. Evolution of the band structure across an ABC. (a) Bands before the gap closing with $m < m_c$. (b–f) Bands at the critical point with $m = m_c$. (g–k) Bands after the gap closing with $m > m_c$. (b, g) For an insulator-to-insulator transition. (c, h) For a transition to a Weyl semimetal protected by $C_{2x,2y}$ or $M_{x,y}$. (d, i) For a transition to a Weyl semimetal protected by $C_{2z}\Theta$. (e, j) For a transition to a Weyl semimetal protected by C_3 together with $C_{2x,2y}$ or $M_{x,y}$. (f, k) For a transition to a nodal line semimetal protected by M_z.

the case of **1p**, we do not specify R_c and R_v since WPs are stable independent of eigenvalue spectra. Here the labels on the Brillouin zone follow the conventions used in Ref. [35], which is illustrated in Appendix D [36].

B. Effective Hamiltonian at the quantum critical point

To describe the effective Hamiltonian at the quantum critical point with $m = m_c$, we redefine the coordinates so that the gap closes at $\mathbf{k} = \mathbf{k}_0 = 0$ and $m = m_c = 0$. As described below, the effective Hamiltonian at the critical point falls into three categories.

First, when there is an insulator-to-insulator transition, the bands disperse linearly in two directions at the critical point, as shown in Fig. 3(b). The relevant effective Hamiltonian is $H = a_1 k_1 \sigma_1 + a_2 k_2 \sigma_2$, where we use k_1, k_2 since they are not along k_x and k_y in general. Second, at the critical point where a pair of WPs is created, the bands disperse linearly in one direction but quadratically in the other direction. In particular, if the WPs are protected by $C_{2x,2y}$ or $M_{x,y}$, the relevant Hamiltonian is $H = a_1 k_y \sigma_1 + a_3 k_1^2 \sigma_3$ [Fig. 3(c)], whereas in the case with $C_{2z}\Theta$, it is $H = a_1 k_1^2 \sigma_1 + (a_2 k_1^2 + a_3 k_2)\sigma_3$ [Fig. 3(d)]. Note that the presence of k_1^2 in the coefficient of σ_3 breaks $k_2 \to -k_2$ symmetry of the energy dispersion. Finally, there are two cases in which the bands disperse quadratically in two directions. One is at the critical point where three pairs of WPs are created [Fig. 3(e)]. The other is at the critical point between an insulator and a nodal line semimetal with the Hamiltonian $H = (a_1 k_1^2 + a_2 k_2^2)\sigma_3$, where we require $a_1 a_2 > 0$ [Fig. 3(f)]. The relevant Hamiltonian is $H = u_1 k^3 \sin 3\theta \sigma_1 + u_{3r} k^2 \sigma_3$, where u_1, u_{3r} are constants and $k_x + i k_y = k e^{i\theta}$. (See Appendix A for the detailed form of the effective Hamiltonian covering $m < m_c$ and $m > m_c$ cases as well.)

III. TOPOLOGICAL CHARGE

In this section, we show that the emergence of stable band degeneracy is always accompanied by a (quantized) topological charge. We define topological charge for each of the three classes of symmetry.

(i) $C_{2z}\theta$: Under time-reversal symmetry, the Berry curvature satisfies $\Omega(-\mathbf{k}) = \Omega(\mathbf{k})$ while under the rotation symmetry, $\Omega(-\mathbf{k}) = \Omega(\mathbf{k})$. Thus, $\Omega(\mathbf{k}) = -\Omega(\mathbf{k})$ under $C_{2z}\theta$, and the Berry curvature vanishes everywhere except for singularities realized by Weyl points [32]. This quantizes the Berry phase in units of π.

(ii) $\{M_z|\mathbf{t}\}$: First, note that eigenvalues are $\pm c$, $|c| = 1$. Following Ref. [8], pick a point $\mathbf{k}_1$ "inside" the loop and another point $\mathbf{k}_2$ "outside" the loop. Define $N_\pm(\mathbf{k}) = N_\pm^c(\mathbf{k}) - N_\pm^v(\mathbf{k})$. Here, $N_\pm^{c(v)}(\mathbf{k})$ is the number of conduction (valence) bands with eigenvalues $\pm c$ at $\mathbf{k}$. The charge is defined to be (see Fig. 4)

$$Q = \frac{\pi}{4}[N_+(\mathbf{k}_1) - N_-(\mathbf{k}_1) - N_+(\mathbf{k}_2) + N_-(\mathbf{k}_2)]. \quad (2)$$

(iii) $\{C_{2x}|\mathbf{t}\}$ (or $\{M_y|\mathbf{t}\}$): The charge is defined exactly as in (2) but with $\mathbf{k}_1$ and $\mathbf{k}_2$ along the symmetry axis with $\mathbf{k}_1$ to the left and $\mathbf{k}_2$ to the right of the gap-closing point. We note that the topological charge can also be defined by integrating along a curve symmetric with respect to the symmetry line. In

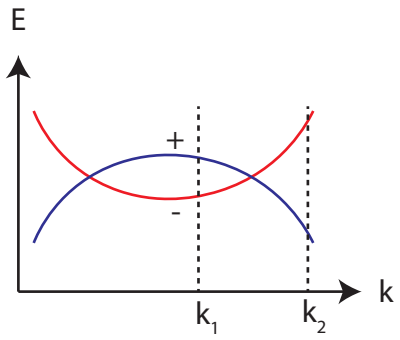

FIG. 4. Schematic diagram of band crossing for cases (ii) and (iii). In case (ii), the k axis is along the line connecting k_1 and k_2, while in case (iii) it is along the symmetry line. The blue (red) band has eigenvalue $+c$ $(-c)$. For the setup in the figure, the charge is π

this case, C_{2x} (or M_y) implies that $\Omega(k_x,k_y) = -\Omega(k_x, -k_y)$ so the integral vanishes unless there is a singularity.

IV. APPLICATION TO 2D MATERIALS

Our theory can be applied to various 2D materials whose band gap is widely tunable by gating, doping, or strain engineering. Let us first focus on the variants of the 2D planar honeycomb lattice, since many 2D materials fall into this category. Because we have organized our results according to LG, it suffices to identify the LG of the lattice structure. The planar honeycomb lattice has the structure of the LG **80**. By distorting the lattice, it is possible to obtain a puckered structure belonging to the LG **42** and a buckled structure with the LG **69** [33,38–42]. Although the planar and the puckered structures contain inversion symmetry, 2D materials are usually fabricated on a substrate, and this breaks inversion symmetry. (One could instead apply electric field normal to the plane of the material.) Then, the symmetry of the planar and the puckered structure is lowered to LG **77** and LG **24**, respectively. Another variant of the honeycomb lattice structure is the dumbbell structure, whose symmetry group, like the planar structure, is also LG **80** [39,40]. Of course, there are also 2D materials whose structure is not based on the honeycomb lattice. For instance, Bi_4Br_4 has the structure belonging to LG **18**, which lowers to LG **13** upon breaking inversion symmetry [43]. HgTe in a HgTe/CdTe quantum well belongs to LG **57** [33]. We summarize the candidate systems and their LGs in Table II. Once the LG for the given material is determined, all possible gap-closing patterns can be read off from Table I.

TABLE II. List of candidate 2D materials. The first column lists the lattice structure. The second column lists the layer group (LG) number for the structure, considering the inversion symmetry breaking effect. The third column lists specific materials that fall under the category.

Structure	LG	Material examples
Planar honeycomb	**77**	Graphene
Puckered honeycomb	**24**	Arsenene [38], antimony [39], bismuth [40], black phosphorus [33]
Buckled honeycomb	**69**	Arsenene [38], blue phosphorous [41], silicon, germanium [42], antimony [39], bismuth [40]
Dumbbell	**77**	Stanene [47], Sn_6Ge_4, $Sn_6Ge_4H_4$ [48]
Bi_4Br_4	**13**	Bi_4Br_4 [43]
HgTe	**57**	HgTe/CdTe heterostructure [33]

V. DISCUSSION

One important application of our classification table is to use it for engineering topological band structure. For instance, recent theoretical and experimental studies on few-layer black phosphorus have shown that it is possible to achieve a transition from an insulator to a Weyl semimetal by doping potassium [33,44,45]. Due to its puckered structure, few-layer black phosphorus under a vertical electric field belongs to LG **24**. Since the gap closing happens on the k_x axis invariant under M_y, $C_{2z}\Theta$, and the M_y eigenvalues of the conduction and valence bands are identical (see Appendix C), the gap-closing pattern should be **1s**, which is confirmed by theoretical studies. Interestingly, a recent theory has shown that such an emergent 2D Weyl semimetal phase can even mediate a transition between a normal insulator and a quantum spin Hall insulator [33].

Moreover, at the critical point for an ABC, unusual fermion dispersion develops, which can generate unconventional quantum critical phenomena. As presented in Sec. II and derived in Appendix A, at the critical point for an insulator-insulator transition, the bands disperse linearly in two directions so that the density of states $D(E) \propto E$. On the other hand, at the critical point where a pair of WP is created, bands disperse linearly in one direction but quadratically in the other direction so that $D(E) \propto \sqrt{E}$. Finally, at the critical point where either a line node or three pairs of WPs are created, bands disperse quadratically in two directions, and therefore, the density of states at the Fermi energy becomes finite. In fact, previous theoretical studies on 2D semimetals with quadratic band crossing have shown the short-range Coulomb interaction is marginally relevant due to the enhanced low energy density of states. Thus, it can induce various insulating phases with broken symmetries [46]. Since such a quadratic dispersion is expected at the critical point in our problem, it is natural to expect novel quantum critical behavior associated with an ABC, which we leave for future study.

ACKNOWLEDGMENTS

S.P. was supported by IBS-R009-D1. B.-J.Y. was supported by IBS-R009-D1, Research Resettlement Fund for the new faculty of Seoul National University, and Basic Science Research Program through the National Research Foundation of Korea (NRF) funded by the Ministry of Education (Grant No. 0426-20150011). B.-J.Y. thanks Shuichi Murakami for useful discussion.

APPENDIX A: GENERAL k·p HAMILTONIAN

As explained in the main text, we may write

$$H = \sum_{i=1}^{3} a_i \sigma_i, \tag{A1}$$

which we will use throughout this section. (We have ignored a term proportional to the 2×2 identity matrix because it does not contribute to the band gap.) Hermiticity of the Hamiltonian requires that and $\mathbf{a} = (a_1,a_2,a_3)$ be real functions of k_1,k_2,m. Let us redefine the coordinates so that the gap closes at $m = 0, \mathbf{k} = (k_1,k_2) = 0$. Also define $\mathbf{q} = (q_1,q_2,q_3) = (k_1,k_2,m)$. With this notation, the gap closes at $\mathbf{q} = 0$. We will sometimes also use k_x, k_y instead of k_1, k_2 when it is more convenient to fix the direction of the coordinates. We will also frequently make use the following property of Pauli matrices.

Suppose that $\sigma_i' = \sum_{j=1}^{3} O_{ij}\sigma_j$ is a set of matrices obtained from the Pauli matrices by an orthogonal transformation $\mathbf{O}$. Then, *if* $H' = \sum_{i=1}^{3} b_i'\sigma_i'$, *the eigenvalues are* $E'_{\pm} = \pm\sqrt{b_1'^2 + b_2'^2 + b_3'^2}$. To show this, note first that the eigenvalues of a Hamiltonian of the form (A1) are $E_{\pm} = \pm\sqrt{a_1^2 + a_2^2 + a_3^2}$. To see this, use the fact that Pauli matrices transform like a vector under SU(2). Thus, there is always an SU(2) transformation that takes the Hamiltonian to $H = \pm\sqrt{a_1^2 + a_2^2 + a_3^2}\sigma_3$, from which the statement follows. Now, using the fact that $\mathbf{O}$ is an orthogonal matrix, $H' = \sum_{i=1}^{3} b_i'\sigma_i' = \sum_{i,j,k=1}^{3} b_k' O_{ik} O_{ij}\sigma_j' = \sum_{i=1}^{3} b_i\sigma_i$, where $b_i = \sum_{k=1}^{3} O_{ik}b_k'$ and $\sigma_i' = \sum_{j=1}^{3} O_{ij}\sigma_j$. Then, it follows that $E'_{\pm} = \pm\sqrt{b_1^2 + b_2^2 + b_3^2} = \pm\sqrt{b_1'^2 + b_2'^2 + b_3'^2}$. Thus, σ_i' obtained from orthogonal transformation of the Pauli matrices are just as good for expanding the Hamiltonian.

1. No symmetry

In this section, we explore in more detail how the gap closes for the case labeled by **f** in the main text. Expanding $\mathbf{a}$ to first order in $\mathbf{q}$ around the gap-closing point, we have $\mathbf{a} = \mathbf{M}\mathbf{q}$. Here, the matrix $\mathbf{M}$ has components $M_{ij} = \frac{\partial a_i}{\partial q_j}$, $i,j = 1,2,3$. We first examine what happens when $\mathbf{M}$ is not invertible. If the matrix has rank 2, the solution is one dimensional in the parameter space, while if the matrix has rank 1, it is two dimensional [49]. Thus, for these cases, a gap-closing solution exists for arbitrary value of m. Since we are assuming that the gap is open when $m < 0$, these cases can be excluded from our consideration. Note that the case $\mathbf{M} = 0$ is unlikely. To see this, carry out the singular value decomposition of $\mathbf{M} = \mathbf{A}^T\mathbf{D}\mathbf{B}$, where $\mathbf{A}$ and $\mathbf{B}$ are orthogonal matrices while $\mathbf{D}$ is diagonal. If $\mathbf{M}$ is not invertible, one or more of the entries of $\mathbf{D}$ is zero, which should not happen without special reason. The conditions we impose on the Hamiltonian, that the gap closes at $m = 0$ but that the gap does not close for $m < 0$, do not give such a constraint. Therefore, we expect $\mathbf{M}$ to be invertible, and in particular, $\mathbf{M} \neq 0$.

Thus, $\mathbf{M}$ is in general invertible, and there is only one solution to the gap-closing condition in the neighborhood of $\mathbf{q} = 0$. This gives a Hamiltonian with linearly dispersing bands which are degenerate at $\mathbf{k} = 0$ when $m = 0$ but quadratically dispersing with a gap when $m \neq 0$. To see this, first write the Hamiltonian as

$$H = \sum_{i,j=1}^{3} M_{ij} q_j \sigma_i. \tag{A2}$$

Carry out the QR decomposition on the matrix $\mathbf{M} = \mathbf{QR}$. Here, $\mathbf{Q}$ is a orthogonal matrix and $\mathbf{R}$ is an upper triangular matrix. Redefine $\sigma_i' = \sigma_j Q_{ji}$ and $q_i' = R_{ij}q_j$ so that $\sum_{ij} M_{ij}q_j\sigma_i = \sum_i q_i'\sigma_i'$. Notice that we may carry out the decomposition such that the diagonal components of $\mathbf{R}$ are positive. This follows because $\det(\mathbf{R}) = R_{11}R_{22}R_{33} \neq 0$, and whenever any one of R_{ii} $(i = 1,2,3)$ is negative, the sign may be absorbed into the matrix $\mathbf{Q}$. For example, if R_{11} is negative, define $\mathbf{D} = diag(-1,1,1)$. Then, $\mathbf{QR} = \mathbf{QDDR}$. The QR decomposition can be carried out with $\mathbf{Q}' = \mathbf{QD}$ and $\mathbf{R}' = \mathbf{DQ}$ instead, in which case R'_{11} is positive. The σ_i' are orthogonal transformations of the Pauli matrices and $\mathbf{q}' = (k_1',k_2',m')$, where k_1' and k_2' are linear transformations of k_1 and k_2, while $m' = cm$ for a positive constant c. The Hamiltonian is then

$$H = k_1'\sigma_1' + k_2'\sigma_2' + m'\sigma_3'. \tag{A3}$$

Now, it is easier to see that the dispersion is linear when $m = cm' = 0$ while the dispersion is quadratic when $m' \neq 0$. Note, however, that this transformation comes with a price that k_1' and k_2' no longer form an orthogonal coordinate system. The gap-closing process is illustrated in Figs. 3(a), 3(b) and 3(g).

When $m = 0$, we can write $\mathbf{a} = \mathbf{L}\mathbf{k}$, where $\mathbf{L}$ is the 3×2 matrix with components $L_{ij} = \frac{\partial a_i}{\partial k_j}$ $(i = 1,2,3$ and $j = 1,2)$. Use the singular value decomposition on $\mathbf{L}$ to write $\mathbf{a} = \mathbf{U}^T\Sigma\mathbf{V}\mathbf{k}$, where $\mathbf{U}$ and $\mathbf{V}$ are orthogonal matrices and Σ is a 3×2 rectangular diagonal matrix with the only nonzero entries $\Sigma_{11} = v_1$, $\Sigma_{22} = v_2$. Defining $\mathbf{a}' = \mathbf{U}\mathbf{a}$ and $\mathbf{k}' = \mathbf{V}\mathbf{k}$, the Hamiltonian can be written as

$$H = v_1k_1'\sigma_1' + v_2k_2'\sigma_2', \tag{A4}$$

where σ_i' is orthogonal transformation of the Pauli matrices.

2. C_{2x} or M_y symmetry

In this section, we carry out a similar analysis for the case labeled **1l** in the main text. As explained in the main text, the requirement for stable band crossing is that $R_c \neq R_v$, where R_c and R_v are the 1D irreducible representations of the symmetry for the conduction and the valence band along the high-symmetry line. This restricts the Hamiltonian to $H = a_3\sigma_3$ on the symmetry lines $k_y = 0,\pi$. Furthermore, off the symmetry axis, $a_{1,2} = k_y b_{1,2}(k_x,k_y^2)$ and $a_3 = a_3(k_x,k_y^2)$ due to the constraint that $H(k_x,-k_y) = C_{2x}H(k_x,k_y)C_{2x}^{-1}$. We can approximate $a_3 = a_{3x}k_x + a_{3yy}k_y^2 + a_{3xx}k_x^2 + a_{3m}m$. We must now implement the condition that there should be no solution for $m < 0$ but that a solution exists for $m = 0$ (along the symmetry line). Setting $k_y = 0$ in a_3, $a_3 = a_{3x}k_x + a_{3xx}k_x^2 + a_{3m}m$. The number of solutions is determined by the discriminant, $D = a_{3x}^2 - 4a_{3xx}a_{3m}m$. Thus, we must have $a_{3x} = 0$ while $a_{3xx}a_{3m} < 0$. Now, make the following expansions: $a_{1,2} = k_y a_{1,2y}$, $a_3 = a_{3xx}k_x^2 + a_{3m}m$. (We do not include k_xk_y because there is a term linear in k_y that will overwhelm k_xk_y when $k_y \neq 0$, while when $k_y = 0$, it is zero. mk_y was ignored for similar reasons.) Thus, the effective Hamiltonian

is

$$H = a_{1y}k_y\sigma_1 + a_{2y}k_y\sigma_2 + (a_{3xx}k_x^2 + a_{3m}m)\sigma_3. \quad \text{(A5)}$$

This describes closing of the gap and the subsequent evolution of Weyl points as shown in Figs. 3(a), 3(c) and 3(h). When $m = 0$, we have $H = k_y a_{1y}\sigma_1 + k_y a_{2y}\sigma_2 + a_{3xx}k_x^2\sigma_3$. Carrying out a rotation in the σ_1, σ_2 space, we find

$$H = a_1' k_y \sigma_1' + a_{3xx}k_x^2\sigma_3. \quad \text{(A6)}$$

Here, the set $(\sigma_1',\sigma_2',\sigma_3)$ is an orthogonal transformation of the Pauli matrices and $a_1' = \sqrt{a_{1y}^2 + a_{2y}^2}$. Note that the dispersion is linear in k_y direction but quadratic in k_x^2 direction [see Fig. 3(c)]. Note also that Weyl points move in the quadratically dispersing direction, which is equivalent to the direction of the high-symmetry line.

3. Space-time inversion

In this section, we carry out a similar analysis for the case **1p** discussed in the main text. As explained in Appendix B 1, we can choose the basis so that the space-time inversion symmetry (STI) $I_{ST} = C_{2z}\theta$ is represented as K, where K is a complex conjugation operator. In such a basis, a_2 will vanish. Expanding about the gap-closing point, $a_1 = M_{1x}k_x + M_{1y}k_y + N_1 m$, $a_3 = M_{3x}k_x + M_{3y}k_y + N_3 m$. The gap-closing condition is that $\mathbf{a} = \mathbf{M}\mathbf{k} + m\mathbf{N} = 0$ [here and in the next section, $\mathbf{a} = (a_1,a_3)$], with $M_{ij} = \frac{\partial a_i}{\partial k_j}$ and $N_i = \frac{\partial a_i}{\partial m}$ where $i = 1,3$ and $j = x,y$. If $\mathbf{M}$ is invertible, there would be a solution for arbitrary m, in contradiction with the assumption that there is no solution for $m < 0$. Thus, $\det\mathbf{M} = 0$ and there exist $\mathbf{n}_1$ such that $\mathbf{M}\mathbf{n}_1 = 0$. Choose $\mathbf{n}_3$ orthogonal to $\mathbf{n}_1$ and expand $\mathbf{k}$ using this basis: $\mathbf{k} = k_1\mathbf{n}_1 + k_2\mathbf{n}_3$. Defining $\mathbf{u}_3 = \mathbf{M}\mathbf{n}_3$, we have $\mathbf{a} = k_2\mathbf{u}_3 + m\mathbf{N}$. There is no k_1 term so we must expand to higher orders. The lowest allowed k_1 term is k_1^2. We include only this term since other higher-order terms will be overwhelmed away from $k_2 = 0$ by terms linear in k_2. Then the lowest order approximation is $\mathbf{a} = \mathbf{u}_{11}k_1^2 + \mathbf{u}_3 k_2 + \mathbf{N}m$.

Now, choose $\hat{\mathbf{u}}_1$ so that $\hat{\mathbf{u}}_1$ and $\hat{\mathbf{u}}_3 = \mathbf{u}_3/|\mathbf{u}_3|$ form an orthonormal basis. Then, we may expand $\mathbf{a}$ in terms of this basis:

$$\begin{aligned}\mathbf{a} &= \mathbf{u}_{11}k_1^2 + \mathbf{u}_3 k_2 + m\mathbf{N}\\ &= [(u_{11})_1\hat{\mathbf{u}}_1 + (u_{11})_3\hat{\mathbf{u}}_3]k_1^2 + u_3 k_2\hat{\mathbf{u}}_3 + m(N_1'\hat{\mathbf{u}}_1 + N_3'\hat{\mathbf{u}}_3).\end{aligned} \quad \text{(A7)}$$

The gap-closing condition $\mathbf{a} = 0$ can be written

$$0 = \begin{pmatrix}(u_{11})_1 & 0\\ (u_{11})_3 & u_3\end{pmatrix}\begin{pmatrix}k_1^2\\ k_2\end{pmatrix} + m\begin{pmatrix}N_1'\\ N_3'\end{pmatrix} = \mathbf{U}\tilde{\mathbf{k}} + m\mathbf{N}. \quad \text{(A8)}$$

This can be solved for $\tilde{\mathbf{k}} = (k_1^2,k_2)$ by inverting the matrix $\mathbf{U} = (\mathbf{u}_{11},\mathbf{u}_3)$: $\tilde{\mathbf{k}} = -m\mathbf{U}^{-1}\mathbf{N} = m\mathbf{Q}$. We require $Q_1 = -N_1'/(u_{11})_1 > 0$ to get a solution for $m \geqslant 0$. To get an expression for the Hamiltonian, notice that choosing $\hat{\mathbf{u}}_1$ and $\hat{\mathbf{u}}_3$ as the basis for expanding $\mathbf{a}$ constitutes a change of basis by an orthogonal matrix $\mathbf{P}^T = (\hat{\mathbf{u}}_1,\hat{\mathbf{u}}_3)$. If we carry out a similar change of basis for the Pauli matrices to get σ_i', the Hamiltonian can be written as $H = \sum_{i=1,3}\sigma_i a_i = \sum_{i,j,k=1,3}\sigma_j P_{ij}P_{ik}a_k = \sum_{i=1,3}\sigma_i' a_i'$. Here, a_i' are components of a_i in the new basis because $\mathbf{P}\mathbf{a} = \mathbf{a}'$. Explicitly,

$$H = \big[(u_{11})_1 k_1^2 + N_1 m\big]\sigma_1' + \big[(u_{11})_3 k_1^2 + u_3 k_2 + N_2 m\big]\sigma_3'. \quad \text{(A9)}$$

This describes gap closing and evolution of Weyl points as shown in Figs. 3(a), 3(d) and 3(i). For $m = 0$, the Hamiltonian can be written as

$$H = (u_{11})_1 k_1^2\sigma_1' + \big[(u_{11})_3 k_1^2 + u_3 k_2\big]\sigma_3'. \quad \text{(A10)}$$

As in the previous case, the energy is linear in k_2 direction but quadratic in k_1 direction. However, this case is slightly different in that there is no $k_2 \to -k_2$ symmetry. The Weyl points move in the quadratically dispersing direction in this case as well. This can be seen from the gap-closing conditions, which are $(u_{11})_1 k_1^2 + N_1 m = 0$ and $(u_{11})_3 k_1^2 + u_3 k_2 + N_2 m = 0$. The former shows that for m slightly greater than 0, $k_1 \approx \sqrt{m}$ and the latter shows that $k_2 \approx m$. Thus, for small m, the Weyl points move predominantly in the quadratically dispersing direction.

4. C_{2x}, $C_{2z}\theta$

We expand on the discussion in the main text in a similar manner with the symmetries C_{2x} and $C_{2z}\theta$, which give rise to either pattern **1l** or pattern **1s**. Since the case for **1l** was discussed in Appendix A 2, we discuss only the case **1s**. For this case, we may take $C_{2x} = i\sigma_0$ and $C_{2z}\theta = K$. (We assumed that the conduction and the valence bands both have eigenvalues $+i$ since the case for eigenvalues $-i$ is similar.) These symmetries restrict the Hamiltonian to $H = a_1\sigma_1 + a_3\sigma_3$, where C_{2x} requires that $a_{1,3}$ be even in k_y. Then, to lowest order, $a_{1,3} = M_{1,3x}k_x + M_{1,3y}k_y^2 + N_{1,3}m$. Explicitly,

$$\begin{aligned}\begin{pmatrix}a_1\\ a_3\end{pmatrix} &= \begin{pmatrix}M_{1x} & M_{1y}\\ M_{3x} & M_{3y}\end{pmatrix}\begin{pmatrix}k_x\\ k_y^2\end{pmatrix} + m\begin{pmatrix}N_1\\ N_3\end{pmatrix}\\ &= \mathbf{M}\tilde{\mathbf{k}} + m\mathbf{N}.\end{aligned} \quad \text{(A11)}$$

Note that we have defined $\tilde{\mathbf{k}} = (k_x,k_y^2)$. Using the QR decomposition, we can write $\mathbf{M} = \mathbf{Q}\mathbf{R}$, where $\mathbf{Q}$ is orthogonal and $\mathbf{R}$ is upper triangular. Rewrite the Hamiltonian as

$$\begin{aligned}H &= \sum_{i=1,2}\sigma_i a_i = \sum_{i,j,k=1,2}\sigma_j Q_{ji}(Q^T)_{ik}a_k\\ &= \sum_{i=1,2}\sigma_i' a_i',\end{aligned} \quad \text{(A12)}$$

where we have defined $\sum_{j=1,2}\sigma_j Q_{ji} = \sigma_i'$ and $\sum_{k=1,2}(Q^T)_{ik}a_k = a_i'$. Noting that $\mathbf{a}' = \mathbf{Q}^T\mathbf{a} = \mathbf{R}\tilde{\mathbf{k}} + m\mathbf{Q}^T\mathbf{N} = \mathbf{R}\tilde{\mathbf{k}} + m\mathbf{N}'$, the Hamiltonian takes the form

$$H = \big(R_{11}k_x + R_{12}k_y^2 + mN_1'\big)\sigma_1' + \big(R_{22}k_y^2 + mN_2'\big)\sigma_3'. \quad \text{(A13)}$$

If we make the correspondence $k_1 \approx k_x$, $k_2 \approx k_y$, this has the form of Eq. (A9). Setting $m = 0$ takes us to (A10). Then, we see that this describes the evolution of a pair of Weyl points symmetrically with respect to the high-symmetry lines $k_y = 0,\pi$.

5. C_3 and C_{2x} or M_1

In this section, we similarly discuss the case labeled **3l** in the main text. The groups **68**, **70**, **76**, and **78** contain threefold rotation about the z axis and twofold rotation or mirror about the in-plane axis as symmetries at the K point. As shown in Appendix B 3, it is possible to create three pairs of Weyl points that evolve from K (KA) point. When this occurs, the representation for C_3 is $-\sigma_0$ and the representation for C_{2x} (M_1) is $\pm i\sigma_3$.

To describe this gap-closing process, it is convenient to use polar coordinates (r,θ) with the K point at $r = 0$. We may also orient our axis so that $\theta = 0$ corresponds to one of the high-symmetry lines. As before, we demand that the gap closes at $m = 0$ while it stays open for $m < 0$. The symmetries of the system imply that $H(r,\theta) = H(r,\theta + 2\pi/3)$ and $H(r,-\theta) = -a_1(r,\theta)\sigma_1 - a_2(r,\theta)\sigma_2 + a_3(r,\theta)\sigma_3$. The former shows that we can Fourier expand in θ while the latter shows that a_1,a_2 are odd and a_3 is even in θ. Expanding the Hamiltonian to lowest order, $H = u_1' r^3 \sin 3\theta\sigma_1 + u_2' r^3 \sin 3\theta\sigma_2 + (u_{3m}m + u_{3r}r^2)\sigma_3$. Note that the analyticity of the Hamiltonian demands that $\sin 3\theta$ should appear with r^3. After performing a rotation in the σ_1, σ_2 space, we may simplify the Hamiltonian as follows:

$$H = u_1 r^3 \sin 3\theta\sigma_1 + (u_{3m}m + u_{3r}r^2)\sigma_3. \tag{A14}$$

Finally, imposing the constraint that there is no gap closing for $m < 0$, we get the constraint $u_{3m}u_{3r} < 0$. This describes closing of the gap and formation of three pairs of Weyl points as shown in Figs. 3(a), 3(e) and 3(j). When $m = 0$, the Hamiltonian is

$$H = u_1 r^3 \sin 3\theta\sigma_1 + u_{3r}r^2\sigma_3. \tag{A15}$$

The dispersion is quadratic in all directions, as can be seen in Fig. 3(j).

6. M_z

Finally, we discuss the case labeled by **loop** in the main text. This corresponds to the case when the eigenvalues of M_z for the conduction and the valence bands are different, which restricts the Hamiltonian to $H = a_3\sigma_3$. Expanding to first order, $a_3 = b_1k_1 + b_2k_2 + a_mm$. The solution space of the gap-closing condition is a plane in the parameter space, which is incompatible with the constraint that there is no solution for $m < 0$. Thus, we include second-order terms, $a_3 = b_1k_1 + b_2k_2 + a_{11}k_1^2 + 2a_{12}k_1k_2 + a_{22}k_2^2 + a_mm$. The extremum for a_3 when $m = 0$ must be 0 at $k_x = k_y = 0$. This condition for extremum gives $b_1 = b_2 = 0$. If we now vary m, there should be a solution for $m > 0$, and it must be a closed loop as we is shown below. Assuming this for now, the solution must be an ellipse for small m. The condition for an ellipse is that $\det(\mathbf{A}) > 0$, where $\mathbf{A}$ is the matrix with components a_{ij}, $i,j = 1,2$. Notice that we may diagonalize this matrix through an orthogonal matrix P. Defining $\mathbf{k}' = P\mathbf{k}$, $a_3 = \lambda_1k_1'^2 + \lambda_2k_2'^2 + a_mm$. The condition for ellipse now reads $\lambda_1\lambda_2 > 0$, while the condition for solution coming into existence for $m \geqslant 0$ becomes $\lambda_1 a_m < 0$

Now, we explain why the solution should be an ellipse. This is because a parabola requires λ_1 or λ_2 to be zero, which is not likely. On the other hand, a hyperbola would be in contradiction with our assumption because there would exist a solution to the gap-closing equation for arbitrary m. Thus, the Hamiltonian is

$$H = \left(\lambda_1k_1'^2 + \lambda_2k_2'^2 + a_mm\right)\sigma_3. \tag{A16}$$

This describes the gap closing and the formation of a line node as illustrated in Figs. 3(a), 3(f) and 3(k). When $m = 0$, the Hamiltonian becomes

$$H = \left(\lambda_1k_1'^2 + \lambda_2k_2'^2\right)\sigma_3. \tag{A17}$$

Thus, the dispersion is quadratic in both directions.

APPENDIX B: CONSIDERATION OF TIME-REVERSAL SYMMETRY

Although time-reversal symmetry fixes only points in the Brillouin zone by itself, it may combine with other crystal symmetries to fix lines or planes. The former occurs when it combines with twofold rotation or mirror symmetry with an in-plane axis, while the latter occurs when it combines with twofold rotation with the axis normal to the plane. We analyze the latter case first, then the former case, and finally, analyze high-symmetry points that are not TRIM. Our goal will be to determine whether consideration of time-reversal symmetry will induce extra double degeneracy, and if not, to determine whether there is any other possible emergent semimetallic phases which were not discussed in detail in the main text. In particular, we discuss the case **3l** in the main text.

1. High-symmetry plane with time-reversal symmetry

In this section, we prove that $C_{2z}\theta = I_{ST}$ can be represented by K, where K is the complex conjugation operator. Because C_{2z} is unitary and θ is antiunitary, I_{ST} must be antiunitary. Thus, $I_{ST} = UK$, where U is an $N \times N$ unitary matrix:

$$UU^\dagger = 1. \tag{B1}$$

Also, the condition $I_{ST}^2 = 1$ implies that

$$UU^* = 1. \tag{B2}$$

These two conditions imply that $U^{-1} = U^\dagger = U^*$. Thus, U is symmetric and unitary and we may write $U = e^{iM}$, where M is symmetric and Hermitian. In other words, M is a real symmetric matrix, and such matrices can be diagonalized by a real orthogonal matrix. Since U transforms under real orthogonal change of basis by matrix O as $U \to OUO^T$, we see that M can be diagonalized to a matrix ϕ with diagonal entries ϕ_n, $n = 1,...,N$. Then, U is transformed to a diagonal matrix $e^{i\phi}$ with diagonal entries $e^{i\phi_n}$, $n = 1,...,N$. Another transformation with matrix $D = diag(e^{-i\phi_1/2},...,e^{-i\phi_n/2})$ gets rid of the phase factors: $e^{i\phi}K \to De^{i\phi}KD^\dagger = K$. Thus, for any set of bands, I_{ST} can be diagonalized, and we may discuss I_{ST} acting on a single energy band (i.e., it does not introduce degeneracy). This means that we may talk about I_{ST} acting on an arbitrary pair of bands as complex conjugation.

2. High-symmetry line with time-reversal symmetry

The analysis for I_{ST} can be applied whenever time reversal is combined with a unitary operator that commutes with it and squares to -1. It is then clear that $C_{2x}\theta$ and $M_y\theta$ also do not enforce double degeneracy. The same comment applies

when C_{2z} is replaced by $\{C_{2z}|ab\}$, because $\{C_{2z}|ab\}^2 = -1$. The analysis becomes more complicated for $\{C_{2x}|ab\}\theta$ and $\{M_y|ab\}\theta$, where $a,b = 0$ or $1/2$. If we denote either of the operators by R, $R^2 = -e^{i2ak_x}$ and $(R\theta)^2 = e^{i2ak_x}$. Writing $\{C_{2x}|ab\}\theta = UK$, we have, in addition to (B1),

$$UU^* = e^{i2ak_x}. \tag{B3}$$

If $a = 0$, the previous analysis applies and there is no degeneracy along the symmetry lines for $\{C_{2x}|ab\}\theta$, namely, the lines $k_x = 0,\pi$. In addition, because the basis can be chosen so that $R\theta = K$, a gap-closing event is not protected along the symmetry line. ($H = a_1\sigma_1 + a_3\sigma_3$, so two equations need to be satisfied for the gap to close while there are two parameters, m and the momentum along the symmetry line.) Since gap closing is not protected off the symmetry line, this does not lead to stable semimetallic phase. On the other hand, if $a = 1/2$, $(R\theta)^2 = -1$, so there is a double degeneracy along the line $k_x = \pi$, but not along the line $k_x = 0$ [50].

Next, consider the possibility of multiple antiunitary symmetry along a line. This happens when there is a simultaneous presence of $C = \{C_{2x}|ab\}\theta$ and $M = \{M_y|a'b'\}\theta$ along the lines $k_x = 0$ or π. If a or a' is $1/2$, there will be a double degeneracy along the lines as we have shown above. If we exclude these cases, they can be diagonalized individually but it is not clear if they can be simultaneously diagonalized. If we set $a = a' = 0$, $CM : (x,y,z,t) \to (x,y+b-b',-z,t)\otimes(-i\sigma_3)$ and $MC : (x,y,z,t) \to (x,y-b+b',-z,t)\otimes(i\sigma_3)$, $CM = -e^{2ik_y(b-b')}MC$. Thus, along the symmetry lines, they either commute or anticommute. Writing $C = U_1K$ and $M = U_2K$, with symmetric and unitary U_1 and U_2, this condition becomes

$$U_1U_2^* = \pm U_2U_1^*. \tag{B4}$$

Now, we showed above that $U_1 = 1$ with a suitable choice of basis, so (B4) implies that in this basis, U_2 is either real or purely imaginary. Because U_2 is symmetric and either U_2 or iU_2 is real, it can be diagonalized by real orthogonal transformation, under which U_1 will remain invariant. Thus, C and M can be simultaneously diagonalized. This analysis could have been carried out by considering the eigenvalues of M_z since $MC \approx M_z$, but this clarifies how the two antiunitary operators can be simultaneously diagonalized. Note that a stable semimetallic phase arises only when $R_c \neq R_v$ for the M_z eigenvalues, which leads to a nodal line, as we already have seen.

We next consider the case when $I_{ST} = C_{2z}\theta$ is present with a nonsymmorphic rotation or mirror with in-plane axis where the translational part is nonzero for the direction normal to the line preserved by the rotation or mirror. In other words, the nonsymmorphic symmetries are of the form $\{C_{2x}|ab\}$ and $\{M_y|ab\}$, where $a = 0$ or $1/2$ and $b = 1/2$. We first note the action of I_{ST} and $\{C_{2x}|ab\}$ on real space and spin space: $I_{ST} : (x,y,z,t)\otimes\sigma_0 \to (-x,-y,z,-t)\otimes i\sigma_1K$ and $\{C_{2x}|ab\} : (x,y,z,t)\otimes\sigma_0 \to (x+a,-y+b,-z,t)\otimes i\sigma_1$. Thus, $\{C_{2x}|ab\}I_{ST} : (x,y,z,t)\otimes\sigma_0 \to (-x+a,y+b,-z,-t)\otimes(-K)$ and $I_{ST}\{C_{2x}|ab\} : (x,y,z,t)\otimes\sigma_0 \to (-x-a,y-b,-z,-t)\otimes K$. Thus,

$$\begin{aligned}\{C_{2x}|ab\}I_{ST} &= -T_{2a,2b}I_{ST}\{C_{2x}|ab\}\\ &= -e^{i(2ak_x-2bk_y)}I_{ST}\{C_{2x}|ab\}.\end{aligned} \tag{B5}$$

Here, $T_{2a,2b}$ is the translation operator with translation in x and y direction by $2a$ and $2b$, respectively.

Now, we examine if I_{ST} doubles the dimension of the representation by examining the eigenvalue of the nonsymmorphic operator. Since $(\{C_{2x}|ab\})^2 = -e^{2iak_x}$, the eigenvectors are $|\pm\rangle$ with eigenvalues $\pm ie^{iak_x}$. The question is whether $I_{ST}|\pm\rangle$ has the same $\{C_{2x}|ab\}$ eigenvalues. Using (B5), $\{C_{2x}|ab\}I_{ST}|\pm\rangle = \pm ie^{i(ak_x-2bk_y)}I_{ST}|\pm\rangle$. Now, it is easy to see that the eigenvalues switch if and only if $b = 1/2$ and $k_y = \pi$ mod 2π. The analysis for mirror symmetry is similar. See, for example, groups **20**, **21**, **24**, **25**. In hindsight, we see that this double degeneracy is actually due to $\{C_{2x}|ab\}\theta$ and $\{M_y|ab\}\theta$, where $a,b = 1/2$ along $k_x = \pi$, but the proof of the double degeneracy is simpler here due to the presence of unitary symmetry whose eigenvalues switch under the action of an antiunitary symmetry. Finally, note that when there is no double degeneracy, the stable semimetallic phase that may arise corresponds to the pattern ii:ij;**1s**,**1l** discussed in the main text. This concludes the analysis of all subtleties that may arise along symmetry lines due to time-reversal symmetry.

3. High-symmetry points that are not TRIM

It is well known that time reversal forces double degeneracy at TRIM and we may exclude these points from our analysis. This leaves us with only K and KA points in the hexagonal Brillouin zone in Fig. 5. There are two questions that need to be addressed. Are there cases when there is no 1D representation at K or KA? If not, can there be the creation of a stable band degeneracy starting from the K or KA point by tuning an external parameter? The answer to the first question is no, as analysis of the inversion asymmetric groups show. The answer to the second question is yes.

We tackle the second question first because this will answer much of the first question. To determine whether stable band degeneracy can evolve from the K point, it helps to notice that protection of Weyl points is due to either I_{ST} or C_{2x} (M_y) type of symmetries when the Weyl points move off the symmetry point.

a. K point in the presence of I_{ST}

This requires the presence of sixfold rotational symmetry in the crystal because there is both C_{2z} and C_3 symmetry. We present the analysis for group **73**, which contains only sixfold rotation in addition to translations. The expectation that the gap closes at K and that I_{ST} will protect the subsequent creation of three pairs of Weyl points is not met.

We showed previously that I_{ST} may be represented by the complex conjugation operator K. On the other hand, the presence of additional symmetry such as C_3 can complicate matters because in the representation where $I_{ST} = K$, C_3 is not in general a diagonal matrix despite the fact that C_3 and $C_{2z}\theta$ commute (because I_{ST} is antiunitary). In fact, operation of C_3 may mix states between different bands, so it may not even be possible to talk about C_3 with an arbitrary pair of bands (because the action of C_3 will take states in one of these two bands into a state from a different band).

To make this clear, begin by finding the eigenvalues of the operator C_3. Since $(C_3)^3 = -1$, the eigenvalues are $e^{i(\pi/3+2\pi n/3)}$ where n is an integer. If it were to be possible to

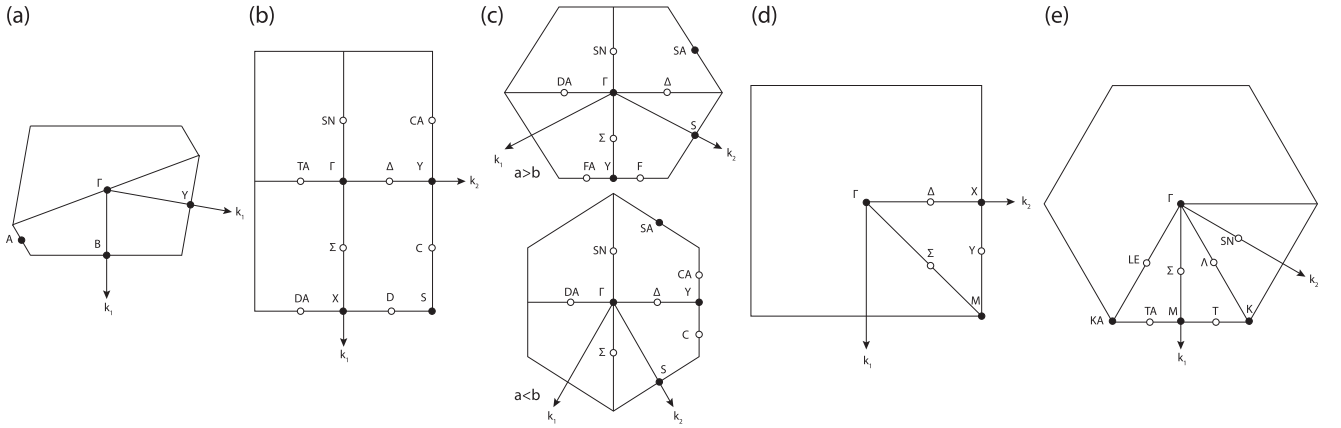

FIG. 5. The schematic figure describing the first Brillouin zone and the relevant high symmetry points and lines for the layer groups. (a) Primitive oblique, (b) primitive rectangular, (c) centered rectangular, (d) primitive square, and (e) primitive hexagonal.

talk about an arbitrary pair of bands so that the pair of bands have C_3 and I_{ST} symmetries, it must be possible to choose representations for these operators so that $I_{ST} = K$ and C_3 has two arbitrary eigenvalues that cubes to -1. We will show below that this is impossible. This implies that an arbitrary pair of energy bands will not simultaneously host I_{ST} and C_3 because both of these are symmetries at K point in the Brillouin zone.

As shown before, we may take $I_{ST} = \sigma_0 K$ for any pair of bands. We find the possible representation for C_3 for an arbitrary pair of bands under the constraint that the action of C_3 does not take us to states outside those in the two bands. The most general form of C_3 is

$$C_3 = \sum_{i=0}^{3} c_i \sigma_i. \tag{B6}$$

Next, we impose the following constraints:

$$[C_3, I_{ST}] = 0, \quad (C_3)^3 = -1, C_3 C_3^\dagger = 1. \tag{B7}$$

We tackle one constraint at a time:

(i) $[C_3, I_{ST}] = 0$: It is easy to see that this condition implies that c_0, c_1, c_3 are real while c_2 is purely imaginary.

(ii) $(C_3)^3 = -1$: Denoting by $\vec{c} = (c_1, c_2, c_3)$, short calculation shows that this gives $c_0^3 + 3c_0\vec{c}^2 = -1$ and $3a_0^2 + \vec{c}^2 = 0$.

(iii) $C_3 C_3^\dagger$: This gives three constraints, $c_0^2 + c_1^2 + c_3^2 - c_2^2 = 1$, $c_0 c_1 + i c_2 c_3 = 0$, and $c_0 c_3 - i c_1 c_2 = 0$.

It follows from $c_0 c_1 + i c_2 c_3 = 0$ and $c_0 c_3 - i c_1 c_2 = 0$ that $c_1 = 0$ or $c_0^2 = c_2^2$. If $c_1 = 0$, the same two conditions show that either $c_3 = 0$ or $c_0 = c_2 = 0$. The latter is impossible because $c_0^2 + c_1^2 + c_3^2 - c_2^2 = 1$ shows that $c_3^2 = 1$ while $3a_0^2 + \vec{c}^2 = 0$ shows that $c_3^2 = 0$. On the other hand, $c_0^2 = c_2^2$ shows that $c_0 = c_2 = 0$ because c_0 is real while c_2 is purely imaginary. The remaining conditions $3a_0^2 + \vec{c}^2 = 0$ and $c_0^2 + c_1^2 + c_3^2 - c_2^2 = 1$ cannot be simultaneously true. Thus, the only possibility is that $c_1 = c_3 = 0$.

If $c_1 = c_3 = 0$, the remaining two conditions are $c_0^3 + 3c_0 c_2^2 = -1$ and $3c_0^2 + c_2^2 = 0$. If $c_2 = 0, c_0 = -1$ while if $c_2 \neq 0, c_0 = \frac{1}{2}$ and $c_2 = \pm i\frac{\sqrt{3}}{2}$.

In conclusion, if $I_{ST} = K$, there are only three possibilities: $C_3 = -\sigma_0, \frac{1}{2}\sigma_0 \pm i\frac{\sqrt{3}}{2}\sigma_2$. Thus, the only allowed pairing of C_3 eigenvalues is $\{-1, -1\}$ and $\{e^{i\pi/3}, e^{-i\pi/3}\}$. In the former case, C_3 does not constrain the form of the Hamiltonian at K point while in the latter case, the two bands are doubly degenerate.

To summarize, suppose that we choose two arbitrary bands. We have shown that it is possible to choose $I_{ST} = K$. However, whether we can speak of C_3 symmetry acting on these two bands depends on the eigenvalues of C_3 at the K point. If it is possible to speak of C_3, the eigenvalues of the two bands must be paired as $\{-1, -1\}$ or $\{e^{i\pi/3}, e^{-i\pi/3}\}$. Otherwise, we must add two additional energy bands to get a four-band model to speak of the C_3 operator.

We note that this can be seen in a different way by examining how the C_3 eigenvalue of a state changes under the operation of I_{ST}. Denote a state having C_3 eigenvalue $e^{i(\pi/3+2\pi n/3)}$ by $|n\rangle$. Then $I_{ST}|n\rangle$ has eigenvalue $e^{-i(\pi/3+2\pi n/3)}$. This means that unless the eigenvalue is -1, I_{ST} imposes double degeneracy. Also, if we want to talk about C_3 and I_{ST} simultaneously on a two-band model, the eigenvalues must be paired as $\{-1, -1\}$ or $\{e^{i\pi/3}, e^{-i\pi/3}\}$, in agreement with the previous analysis.

b. K point in the presence of C_{2x} or M_1 type of symmetry

The simplest case is when there is only the threefold rotation and C_{2x} or M_1 (twofold rotation or mirror whose symmetry axis passes through the K point), as in groups **68** and **70**, respectively. The 1D representation for C_3 is -1, while those for twofold rotation or mirror is $\pm i$. This is due to the relation $C_3 P = P C_3^{-1}$, where P is either C_{2x} or M_y, which implies that unless a state has eigenvalue -1 for C_3, the representation cannot be one dimensional.

For two pairs of energy bands whose C_3 eigenvalue is -1 at the K point, it is the eigenvalues of P that determine whether bands may close at the high-symmetry point. If $R_c = R_v$ for P, the gap does not close at the K point in general because $P \propto \sigma_0$, but it may close if $R_c \neq R_v$ because $P \propto \sigma_3$. After the gap closes, there will be evolution of three pairs of Weyl points along the three high-symmetry lines that cross at the K point because $R_c \neq R_v$ along these lines and the problem reduces to **1l** discussed in the main text. This pattern of gap closing is labeled **3l**. Note that the mechanism for protection of Weyl points in this case is the same as that for C_{2x} or M_y.

TABLE III. Layer groups organized according to their Bravais lattice.

Brillouin zone	Layer group
Oblique p	**1**, **3**, **4**, **5**
Rectangular p	**8**, **9**, **11**, **12**, **19**, **20**, **21**, **23**, **24**, **25**, **27**, **28**, **29**, **30**, **31**, **32**, **33**, **34**
Rectangular c	**10**, **13**, **22**, **26**, **35**, **36**,
Square p	**49**, **50**, **53**, **54**, **55**, **56**, **57**, **58**, **59**, **60**
Hexagonal p	**65**, **67**, **68**, **69**, **70**, **73**, **74**, **76**, **77**, **78**, **79**

Next, we discuss the case with C_3 replaced by C_6 symmetry, which is equivalent to considering an additional I_{ST} symmetry at the K point. This occurs for **76** and **77**, which contain C_{2x} or M_1, respectively, in addition to C_3 and I_{ST} at the K point. From the above analysis, the only 1D representation possible is $C_3 = -1$ and $P = \pm i$, where $P = C_{2x}$ or M_1. The claim is that I_{ST} does not force degeneracy. This is easy to see because we have already shown in Appendix B 2 that the group relation between I_{ST} and P is consistent with the representation, and we have shown in the previous section that the group relation between I_{ST} and C_3 is consistent with the representation, and finally, we have shown in this section that the group relation between C_3 and P is consistent with the representation. The conclusion follows by observing that C_3, P, and I_{ST} generate the group.

Now, **76** contains **68** as a subgroup, and **77** contains **70** as a subgroup. Restricting the representation for **76** and **77** to these subgroups, we obtain the representation for **68** and **70** that was found previously. Thus we see then that if $R_c = R_v$ for P, the gap does not close at K, while if $R_c \neq R_v$, it is possible to obtain **3l**.

c. Possibility of additional double degeneracy at the K point

Now, we come back to the question of whether consideration of time-reversal symmetry can forbid a one-dimensional representation at the K point. We begin by listing all of the possible symmetries:

$$C_3, M_2, C_{2x}, M_z, M_x\theta, C_{22}\theta, I_{ST}. \tag{B8}$$

Here, M_2 and C_{2x} is a mirror symmetry or twofold rotation symmetry that leaves invariant one of the high-symmetry lines passing through the K point. [They fix the line LE passing through the KA point in Fig. 5(e).] Note that we have not listed symmetries that can be formed by combining one of the symmetries we have listed with C_3, which will always be present for the hexagonal Brillouin zone. For example, M_1 and M_3, which are also mirror symmetries that leave invariant one of the high-symmetry lines passing through the K point, are not listed because they can be obtained by a suitable combination of M_2 and C_3. Note also that C_{22} is a twofold rotation symmetry and M_x is a mirror symmetry fixing the line SN in Fig. 5(e). It can be shown by going through all of the combinations that it suffices to consider only the following symmetries in addition to C_3 at the K point:

$$(M_x\theta), (C_{22}\theta), (I_{ST}), (M_1, I_{ST}), (C_{2x}, I_{ST}), (C_{22}\theta, M_x\theta). \tag{B9}$$

Note that the combination is such that there is no inversion symmetry, and time-reversal symmetry appears in combination with some spatial symmetry. Before moving on, we note that there does exist one case where there is no 1D irrep because of the simultaneous presence of M_2 and C_{2x}, which has been discussed in the main text (see group **79**).

We have actually carried out most of the calculations needed to determine that addition of time-reversal symmetry to the system does not prohibit 1D representation at the K point. The presence of $C_{22}\theta$ or $M_x\theta$ in addition to C_3 appears as a subgroup of **76** and **77**, respectively. This leaves us with the case with $C_{22}\theta, M_x\theta$. However, we have already shown that it is possible to simultaneously diagonalize these symmetries, which means it is possible to talk about these symmetries acting on one band. In general, we may take $C_{22}\theta = K$, $M_x\theta = \pm iK$ to satisfy (B4). A candidate representation for C_3 is -1. We have shown that this representation is consistent with the group relation between $C_{22}\theta$ and C_3. If $M_x\theta = K$, our previous calculation would show that this is also consistent with $C_3 = -1$. However, the phase factor in front of K is irrelevant for the group relation between $M_x\theta$ and C_3. This concludes the proof.

APPENDIX C: BLACK PHOSPHOROUS

In this section, we present a simple application to the k·p model of black phosphorous. As shown in Ref. [33], the **k·p** Hamiltonian near the Γ point takes the form

$$H(k_x, k_y) = Ak_x\sigma_y + \left(M - B_1k_x^2 - B_2k_y^2\right)\sigma_z + \lambda_1 s_y\sigma_y + \lambda_2 k_y s_z\sigma_x. \tag{C1}$$

Here, s_i and σ_i are the Pauli matrices for spin and orbital degrees of freedom, respectively, M is a tunable parameter, and $A, B_1, B_2, \lambda_1, \lambda_2$ are constants. Black phosphorous has a puckered structure, and when the symmetry is lowered by breaking the inversion symmetry, it belongs to layer group **24**, which contains M_x and M_y symmetries (note that $M_xM_y \approx C_{2z}$). Although the mirror symmetries are nonsymmorphic, this is irrelevant for k·p theory near the Γ point. Taking this into account, the symmetries take the following representations:

$$M_x = is_x\sigma_z, M_y = is_y, \theta = is_yK. \tag{C2}$$

Here, θ is the usual time-reversal symmetry. As we tune the parameter M, the gap may close or open along $k_x = 0$ or $k_y = 0$. Our claim is that this gap closing follows the pattern **1s**. As an example, we verify this along $k_y = 0$, along which M_y is a symmetry. In particular, we show that the M_y eigenvalues for the gap-closing bands are equal. To do this, set $k_y = 0$ in the Hamiltonian to get

$$H(k_x, k_y) = Ak_x\sigma_y + \left(M - B_1k_x^2\right)\sigma_z + \lambda_1 s_z\sigma_y. \tag{C3}$$

Notice that we have changed the basis in the spin sector so that $s_y \to s_z$. In this basis, $M_y = is_z$. Now, it is easy to see that the gap closes between bands in the sector with the same s_z eigenvalues, which means that the M_y eigenvalues are equal for the bands that cross.

APPENDIX D: BRILLOUIN ZONE

For the reader's convenience, we have organized the layer groups according to their Brillouin zone in Table III and illustrated the Brillouin zone in Fig. 5 with the convention used by Litvin and Wike [35].

[1] S. M. Young, S. Zaheer, J. C. Y. Teo, C. L. Kane, E. J. Mele, and A. M. Rappe, Dirac Semimetal in Three Dimensions, Phys. Rev. Lett. **108**, 140405 (2012).

[2] J. A. Steinberg, S. M. Young, S. Zaheer, C. L. Kane, E. J. Mele, and A. M. Rappe, Bulk Dirac Points in Distorted Spinels, Phys. Rev. Lett. **112**, 036403 (2014).

[3] Z. Wang, Y. Sun, X. Q. Chen, C. Franchini, G. Xu, H. Weng, X. Dai, and Z. Fang, Dirac semimetal and topological phase transitions in A_3Bi (A=Na, K, Rb), Phys. Rev. B **85**, 195320 (2012).

[4] Z. Wang, H. Weng, Q. Wu, X. Dai, and Z. Fang, Three-dimensional Dirac semimetal and quantum transport in Cd_3As_2, Phys. Rev. B **88**, 125427 (2013).

[5] B.-J. Yang and N. Nagaosa, Classification of stable three-dimensional Dirac semimetals with nontrivial topology, Nat. Commun. **5**, 4898 (2014).

[6] B.-J. Yang, T. Morimoto, and A. Furusaki, Topological charges of three-dimensional Dirac semimetals with rotation symmetry, Phys. Rev. B **92**, 165120 (2015).

[7] Z. K. Liu, B. Zhou, Y. Zhang, Z. J. Wang, H. M. Weng, D. Prabhakaran, S.-K. Mo, Z. X. Shen, Z. Fang, X. Dai, Z. Hussain, and Y. L. Chen, Discovery of a three-dimensional topological Dirac semimetal, Na_3Bi, Science **343**, 864 (2014).

[8] B.-J. Yang, T. A. Bojesen, T. Morimoto, and A. Furusaki, Topological semimetal protected by off-centered symmetries in nonsymmorphic crystals, Phys. Rev. B **95**, 075135 (2017).

[9] M. Neupane, S.-Y. Xu, R. Sankar, N. Alidoust, G. Bian, C. Liu, I. Belopolski, T.-R. Chang, H.-T. Jeng, H. Lin, A. Bansil, F. Chou, and M. Z. Hasan, Observation of a three dimensional topological Dirac semimetal phase in high-mobility Cd_3As_2, Nat. Commun. **5**, 3786 (2014).

[10] S. Borisenko, Q. Gibson, D. Evtushinsky, V. Zabolotnyy, B. Büchner, and R. J. Cava, Experimental Realization of a Three-Dimensional Dirac Semimetal, Phys. Rev. Lett. **113**, 027603 (2014).

[11] S. Jeon, B. B. Zhou, A. Gyenis, B. E. Feldman, I. Kimchi, A. C. Potter, Q. D. Gibson, R. J. Cava, A. Vishwanath, and A. Yazdani, Landau quantization and quasiparticle interference in the three-dimensional Dirac semimetal Cd_3As_2, Nat. Mater. **13**, 851 (2014).

[12] Z. K. Liu, J. Jiang, B. Zhou, Z. J. Wang, Y. Zhang, H. M. Weng, D. Prabhakaran, S.-K. Mo, H. Peng, P. Dudin, T. Kim, M. Hoesch, Z. Fang, X. Dai, Z. X. Shen, D. L. Feng, Z. Hussain, and Y. L. Chen, A stable three-dimensional topological Dirac semimetal Cd_3As_2, Nat. Mater. **13**, 677 (2014).

[13] X. Wan, A. M. Turner, A. Vishwanath, and S. Y. Savrasov, Topological semimetal and Fermi-arc surface states in the electronic structure of pyrochlore iridates, Phys. Rev. B **83**, 205101 (2011).

[14] A. A. Burkov and L. Balents, Weyl Semimetal in a Topological Insulator Multilayer, Phys. Rev. Lett. **107**, 127205 (2011).

[15] C. Fang, M. J. Gilbert, X. Dai, and B. A. Bernevig, Multi-Weyl Topological Semimetals Stabilized by Point Group Symmetry, Phys. Rev. Lett. **108**, 266802 (2012).

[16] H. Weng, C. Fang, Z. Fang, B. A. Bernevig, and X. Dai, Weyl Semimetal Phase in Noncentrosymmetric Transition-Metal Monophosphides, Phys. Rev. X **5**, 011029 (2015).

[17] S. M. Huang, S. Y. Xu, I. Belopolski, C. C. Lee, G. Chang, B. K. Wang, N. Alidoust, G. Bian, M. Neupane, C. Zhang, S. Jia, A. Bansil, H. Lin, and M. Z. Hasan, A Weyl Fermion semimetal with surface Fermi arcs in the transition metal monopnictide TaAs class, Nat. Commun. **6**, 7373 (2015).

[18] B. Q. Lv, H. M. Weng, B. B. Fu, X. P. Wang, H. Miao, J. Ma, P. Richard, X. C. Huang, L. X. Zhao, G. F. Chen, Z. Fang, X. Dai, T. Qian, and H. Ding, Experimental Discovery of Weyl Semimetal TaAs, Phys. Rev. X **5**, 031013 (2015).

[19] S.-Y. Xu *et al.*, Discovery of a Weyl fermion semimetal and topological Fermi arcs, Science **349**, 613 (2015).

[20] B. Q. Lv *et al.*, Observation of Weyl nodes in TaAs, Nat. Phys. **11**, 724 (2015).

[21] L. X. Yang, Z. K. Liu, Y. Sun, H. Peng, H. F. Yang, T. Zhang, B. Zhou, Y. Zhang, Y. F. Guo, M. Rahn *et al.*, Weyl semimetal phase in the non-centrosymmetric compound TaAs, Nat. Phys. **11**, 728 (2015).

[22] H. Watanabe, H. C. Po, M. P. Zaletel, and A. Vishwanath, Filling-Enforced Gaplessness in Band Structures of the 230 Space Groups, Phys. Rev. Lett. **117**, 096404 (2016).

[23] J. Kruthoff, J. de Boer, J. van Wezel, C. L. Kane, and R.-J. Slager, Topological classification of crystalline insulators through band structure combinatorics, arXiv:1612.02007.

[24] S. Murakami, Phase transition between the quantum spin Hall and insulator phases in 3D: Emergence of a topological gapless phase, New J. Phys. **9**, 356 (2007).

[25] S. Murakami and S.-I. Kuga, Universal phase diagrams for the quantum spin Hall systems, Phys. Rev. B **78**, 165313 (2008).

[26] C. L. Kane and E. J. Mele, Quantum Spin Hall Effect in Graphene, Phys. Rev. Lett. **95**, 226801 (2005).

[27] C. L. Kane and E. J. Mele, Z_2 Topological Order and the Quantum Spin Hall Effect, Phys. Rev. Lett. **95**, 146802 (2005).

[28] S. M. Young and C. L. Kane, Dirac Semimetals in Two Dimensions, Phys. Rev. Lett. **115**, 126803 (2015).

[29] B. J. Wieder and C. L. Kane, Spin-orbit semimetals in the layer groups, Phys. Rev. B **94**, 155108 (2016).

[30] Because degeneracy due to time-reversal symmetry along high-symmetry points or lines is not tabulated for layer groups in Ref. [35], we have analyzed the issue in detail in Appendix B.

[31] S. Murakami, M. Hirayama, R. Okugawa, and T. Miyake, Emergence of topological semimetals in gap closing in semiconductors without inversion symmetry, Sci. Adv. **3**, e1602680 (2017).

[32] C. Fang and L. Fu, New classes of three-dimensional topological crystalline insulators: Nonsymmorphic and magnetic, Phys. Rev. B **91**, 161105(R) (2015).

[33] J. Ahn and B.-J. Yang, Unconventional Topological Phase Transition in Two-Dimensional Systems with Space-Time Inversion Symmetry, Phys. Rev. Lett. **118**, 156401 (2017).

[34] E. Hitzer and D. Ichikawa, Representation of crystallographic subperiodic groups by geometric algebra, *Electronic Proc. of AGACSE 3, Leipzig, Germany, 17-19 Aug.* (2008).

[35] D. B. Litvin and T. R. Wike, *Character Tables and Compatibility Relations of The Eighty Layer Groups and Seventeen Plane Groups* (Plenum Press, New York, 1991).

[36] A caveat is in order: the group numbers used in Ref. [37] differs from those used in Ref. [35]. The relation between these conventions can be found in Ref. [51].

[37] *International Tables for Crystallography*, 2nd ed., edited by V. Kopsky and D. B. Litvin (Elsevier, New York, 2010), Vol E.

[38] C. Kamal and M. Ezawa, Arsenene: Two-dimensional buckled and puckered honeycomb arsenic systems, Phys. Rev. B **91**, 085423 (2015).

[39] G. Zheng, Y. Jia, S. Gao, and S.-H. Ke, Comparative study of thermal properties of group-VA monolayers with buckled and puckered honeycomb structures, Phys. Rev. B **94**, 155448 (2016).

[40] T. Nagao, J. T. Sadowski, M. Saito, S. Yaginuma, Y. Fujikawa, T. Kogure, T. Ohno, Y. Hasegawa, S. Hasegawa, and T. Sakurai, Nanofilm Allotrope and Phase Transformation of Ultrathin Bi Film on Si(111)-7×7, Phys. Rev. Lett. **93**, 105501 (2004).

[41] Z. Zhu and D. Tománek, Semiconducting Layered Blue Phosphorus: A Computational Study, Phys. Rev. Lett. **112**, 176802 (2014).

[42] S. Cahangirov, M. Topsakal, E. Aktürk, H. Şahin, and S. Ciraci, Two- and One-Dimensional Honeycomb Structures of Silicon and Germanium, Phys. Rev. Lett. **102**, 236804 (2009).

[43] J.-J. Zhou, W. Feng, C.-C. Liu, S. Guan, and Y. Yao, Large-gap quantum spin Hall insulator in single layer bismuth monobromide Bi_4Br_4, Nano Lett. **14**, 4767 (2014).

[44] J. Kim, S. S. Baik, S. H. Ryu, Y. Sohn, S. Park, B.-G. Park, J. Denlinger, Y. Yi, H. J. Choi, and K. S. Kim, Observation of tunable band gap and anisotropic Dirac semimetal state in black phosphorus, Science **349**, 723 (2015).

[45] S. S. Baik, K. S. Kim, Y. Yi, and H. J. Choi, Emergence of Two-Dimensional Massless Dirac Fermions, Chiral Pseudospins, and Berry's Phase in Potassium Doped Few-Layer Black Phosphorus, Nano Lett. **15**, 7788 (2015).

[46] K. Sun, H. Yao, E. Fradkin, and S. A. Kivelson, Topological Insulators and Nematic Phases from Spontaneous Symmetry Breaking in 2D Fermi Systems with a Quadratic Band Crossing, Phys. Rev. Lett. **103**, 046811 (2009).

[47] P. Tang, P. Chen, W. Cao, H. Huang, S. Cahangirov, L. Xian, Y. Xu, S.-C. Zhang, W. Duan, and A. Rubio, Stable two-dimensional dumbbell stanene: A quantum spin Hall insulator, Phys. Rev. B **90**, 121408(R) (2014).

[48] X. Chen, L. Li, and M. Zhao, Hydrogenation-induced large-gap quantum-spin-Hall insulator states in a germanium–tin dumbbell structure, RSC Adv. **5**, 72462 (2015).

[49] Let $\mathbf{M}$ be an $m \times n$ matrix. The rank of $\mathbf{M}$ is the number of independent rows, which is equivalent to the number of independent columns. The nullity of $\mathbf{M}$ is the dimension of the solution space of the linear equation $\mathbf{Mv} = 0$. The rank-nullity theorem states that the rank of $\mathbf{M}$ and the nullity of $\mathbf{M}$ adds up to n.

[50] It can be shown [52] that if an antiunitary operator A satisfies $A^2 = e^{i\phi}$, it can be diagonalized if $e^{i\phi} = 1$, while it can only be block diagonalized with 2×2 matrices of the form $\cos\frac{\phi}{2}\sigma_1 - \sin\frac{\phi}{2}\sigma_2$ along the diagonal if $e^{i\phi} \neq 1$.

[51] V. Kopsky and D. B. Litvin, Nomenclature, Symbols and Classification of the Subperiodic Groups (1991).

[52] S. Weinberg, *The Quantum Theory of Fields Volume 1: Foundations* (Cambridge University Press, Cambridge, UK, 2005).